ASTEC validation of sfp dewatering using results from the denopi project

L. Laborde, Benoît Migot

ASTEC VALIDATION OF SFP DEWATERING USING RESULTS FROM THE DENOPI PROJECT

Laborde L. and Migot B.
Institut de Radioprotection et de Sûreté Nucléaire (IRSN),
Centre de Cadarache B.P. 3, 13115 Saint-Paul-lez-Durance Cedex, France
laurent.laborde@irsn.fr; benoit.migot@irsn.fr

ABSTRACT

Loss of cooling in a Spent Fuel Pool (SFP) of a nuclear power plant can lead to the melting of fuel assemblies and to strong radiological consequences to the environment. In order to study the first phases of such accidents, up to the fuel assemblies uncovery, the DENOPI project was launched by the French Institute for Radiation Protection and Nuclear Safety (IRSN) supported and funded by the French Government and partners. Among the different facilities developed in the project, the MIDI facility aims at studying the complex thermal-hydraulics phenomena occurring in a large water pool heated from the bottom by electrical rods arranged in dedicated racks. MIDI is scaled by homothety to a typical French SFP. Different assembly arrangements (loading patterns) have been tested at different power levels, with either uniform power repartition, or hot and cold cells. In each test, the water level and temperatures at different elevations are followed, as well as mass flow rate entering each fuel rack. These experimental results also provide relevant data for the analysis and understanding of large natural convection loops that are expected in immersed passive heat removal systems of Small Modular Reactors. The forthcoming OECD/NEA POLCA project aims to extend such results database, in particular to assess the capability of thermal-hydraulics codes to reproduce the main tendencies of these experimental results.
The ASTEC code developed by IRSN is a system code dedicated to the simulation of major accidents in nuclear facilities that may lead to the release of radiological material. Recent works within the MUSA European project have shown the importance of reducing models uncertainties in the first phases of the accident, during the pool dewatering. In this paper, first simulations of MIDI tests are performed with ASTEC in order to assess and improve the capability of ASTEC to simulate the dewatering of a large water pool such as a SFP during a loss-of-cooling accident. Simulations are performed for a selection of MIDI tests with different heating patterns and power levels. Different models of subcooled boiling models from the literature are tested in ASTEC, stressing the key role of these models for an accurate prediction of the experimental flow.

KEYWORDS
Spent Fuel Pool, Loss-of-Cooling, ASTEC, subcooled boiling, natural convection.

1 INTRODUCTION

Since the Fukushima Daiichi accident that occurred in Japan in 2011, nuclear safety in Spent Fuel Pools (SFP) has become a major issue. Among the main concerns are Loss-of-Cooling Accidents (LOCA) which can lead to the dewatering of the pool and, without any mitigation, to the fuel assemblies uncovery and degradation, with a large release of fission products to the environment. In order to improve our understanding of such accidents, the Organisation for Economic Cooperation and Development (OECD) launched several research activities and published in 2018 a Phenomena Identification Ranking Table (PIRT) [1] identifying the physical phenomena that are of high importance and high uncertainty. A recent

update of the progresses performed after this PIRT can be found in [2]. One of the identified priorities is to improve the capability of computer codes to simulate such accidents, and in particular the first phase of the accident, up to the fuel assemblies uncovery. Due to the turbulent nature of the natural convection-driven flow in the large open region above the fuel, such calculations are usually performed using Computational Fluid Dynamic (CFD) codes [3, 4, 5]. However, such calculations are very expensive, in particular when it comes to two-phase flows. Therefore, studies are also performed with 1D thermal-hydraulic system codes [6, 7] which provide much faster but less accurate results, due to the rough nodalizations and approximations applied in these codes.
Recent works have also tested the ASTEC severe accident code in a 2D application to model the water evaporation of a small container [8], stressing the difficulty to use these codes to model such turbulent flow in open regions.
In addition, recent simulations performed with severe accident codes like ASTEC or MELCOR in the MUSA project [9] also underlined difficulties in modelling the fuel assembly uncovery phase: in such stratified flows with a very thin two-phase region due to the low decay heat, periodic increases of the evaporation mass flow rate were observed, in relation with the nodalization, which led to periodic fuel cooling, delaying in some cases the fission products release.
Beyond these current difficulties, one of the main limitations of these simulation tools for SFP applications comes from the lack of relevant validation data: these codes are in general applied in conditions corresponding to reactor transients, with high pressure and high heat fluxes, for which the codes are well validated. In contrast, SFP transients occur close to the atmospheric pressure with very low decay heat, so that the validation of these tools to this low pressure and heat flux range is of crucial importance.
Therefore, to extend the validation database of thermal-hydraulic codes and to improve the understanding of phenomena involved in SFP accidents prior to the severe accident phase, the DENOPI project was launched in 2013 by IRSN. Funded by the French Government, the project consists in experimental work organized in three axes corresponding to different scales and consecutive phases of the accident [10]:

- large-scale study of SFP dewatering before fuel uncover (MIDI device);
- mid-scale observation of assembly uncovery before fuel degradation (ASPIC device);
- small-scale analysis of fuel cladding oxidation in SFP-LOCA.

The current paper is focused on the first axis and makes use of data recently obtained in the MIDI mock-up located at Cadarache (France). First, the MIDI experimental device is quickly described, together with the series of tests and main results. Then, calculations using the severe accident code ASTEC are presented, for different loading patterns and power levels. The influence of several subcooled boiling models from the literature is also presented. The objective of this work is two-fold: to improve the modelling and results of current version of ASTEC for SFP applications, and to identify the limitations and needs for further experimental data and models, with the idea to apply ASTEC to more generic open regions applications like immersed passive heat removal systems of Small Modular Reactors.

2 MIDI EXPERIMENTAL DEVICE

2.1 Description of the MIDI mock-up

The MIDI mock-up consists in a large rectangular basin of water representing a typical French PWR SFP, with a 1/36 ratio for the free surface and 1/3 ratio for pool height. A scheme of the MIDI device is represented in Figure 1 and the main characteristics of the installation are indicated in Table I. The basin is heated by 21 heating elements located at the bottom of the device, representing 21 cells of a storage rack, each element being composed of a 3x3 electrically heated rod bundle. The 21 cells are separated by solid walls representing the racks, so that horizontal flows between cells are not possible in the heated region. Further details of the facility can be found in [10]. One key feature of MIDI is the possibility to modulate the heating power of each cell individually, simulating different arrangements of hot and cold assemblies in a SFP. The

four loading patterns already tested are indicated in Figure 2. Above the pool, a ventilation hood extracts the steam outside the building.

MIDI is equipped with a large number of sensors to characterize the flows in the racks and in the pool. Temperatures are measured at different elevations of the pool (with uncertainties below 1 degree), above hot and cold assemblies and at the inlet and outlet of the cells. Mass flow rates are measured in each heated cell using vane wheel flow sensors (with an accuracy of 7.5% and a sensitivity limit of 0.5 kg/s) while the water level is recorded using a pressure gauge and a guided level–radar probe. The flow in the pool can be visualized and recorded thanks to cameras looking through dedicated optical windows at several elevations of the tank. The atmosphere of the pool, maintained at 1 bar, is also monitored: gas temperature, total pressure and relative humidity above the free surface are measured.

The current MIDI test matrix is built on varying the following parameters:

- Overall heating power up to 300 kW (with a local maximum power of 50 kW per cell);
- Loading pattern as indicated in Figure 2;
- Initial water level: 4 m or 2 m.

Each test follows a 3-phases protocol: basin fill-up to the required level, heat up of the pool to 50°C by the heating elements with a forced convection, stop of the forced convection and start of the experimental test by application of the loading pattern. Tests are stopped when the remaining collapsed level reaches 50 cm above the top of the racks.

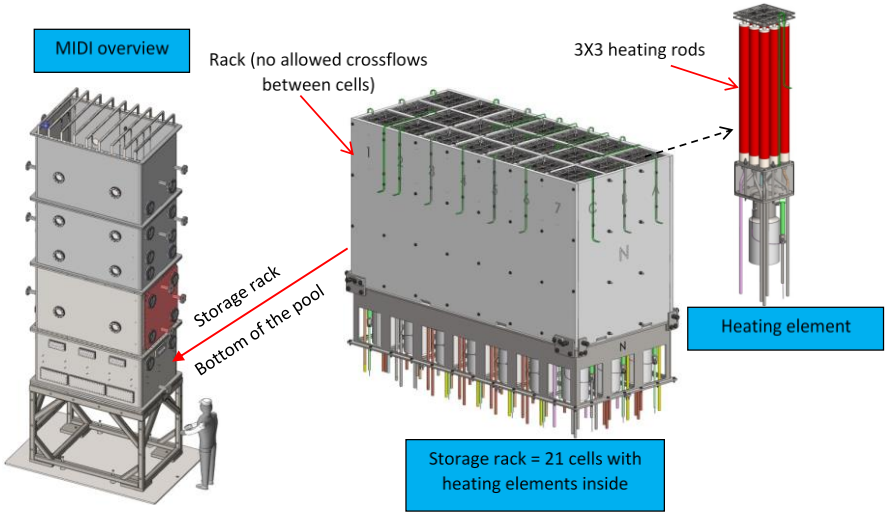

Figure 1: MIDI facility

Table I: Main parameters of the MIDI facility

Parameters	MIDI facility
Maximum water level (m)	4.0
Bundle active length (m)	0.7
Basin width (m)	1.35
Basin length (m)	2.10
Overall rack flow section (m^2)	0.65
Free surface area (m^2)	2.835
Bundle width (m)	0.225
Bundle porosity (-)	0.61
Number of cells (-)	21 (7 X3)
Power range (kW)	[50;300]
Max. power per bundle (kW)	50
Volumetric power (kW/m^3)	[4.2;25.1]

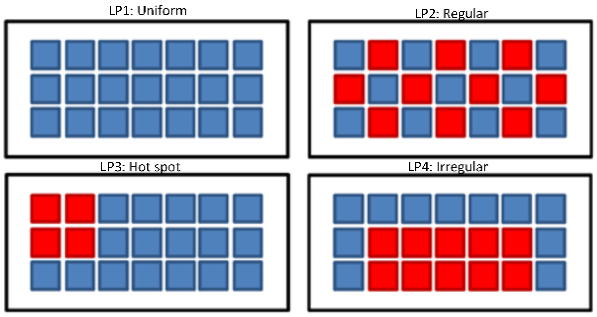

Figure 2: Loading patterns applied in MIDI tests.

2.2 Main Results of MIDI Experiments

The first MIDI campaign included nine different tests, of which 5 have been run twice, successfully checking the repeatability of the tests. Only the main conclusions of the tests are reported in this section, while time evolutions of temperature and mass flow rate in the cells are provided in the next section, together with ASTEC results. The tests have put in evidence a phenomenology consisting in three consecutive phases corresponding to three vaporization modes.

At first, while the temperature at the pool surface is below saturation, vaporization is driven by evaporation at the free surface. Then, as soon as the pool temperature reaches the local saturation temperature, flashing of uprising overheated water occurs. During this phase, the water temperature at the rack outlet is significantly lower than the saturation temperature at the top of the racks, due to the hydrostatic pressure above the racks, preventing water boiling in this region. At this stage, local boiling may appear on the heated elements, but bubbles quickly recondensate when water is mixed with cooler liquid above the racks. When the water level approaches 1m above the top of the racks, the local saturation temperature has decreased down to the temperature at the outlet of the cells, so that the boiling phase starts, with a continuous bubble plume from the top of the racks to the free surface.

It was observed that the effect of the loading pattern was only significative in the vicinity of the cells or inside the racks. With the “Hot spot” pattern, the presence of a significantly hotter plume above the heating zone was reported, promoting the formation of vapor bubbles by flashing in this zone. For other patterns, the temperature in the pool is homogeneous except at the outlet of cells with power higher than 4 kW.

3 ASTEC MODELLING OF MIDI TESTS

3.1 Main Characteristics of ASTEC V3.1.1 Code

The severe accident integral code ASTEC [11, 12] developed by IRSN aims at simulating an entire severe accident sequence in nuclear facilities, from the initiating event up to the release of radioactive elements in the atmosphere. Compared to the last versions of the V2 series, the current V3 series of ASTEC covers additional applications like accidents in fuel reprocessing facilities, while previous applications related to water-cooled reactors remain globally unchanged. The software is organized in modules in charge of different regions and physics of the represented nuclear facility. In this work, the only ASTEC relevant modules are ICARE, in charge of heat transfers and degradation in a reactor core or SFP, and CESAR, which deals with the thermal-hydraulics in the core and circuits. The CESAR module [13] is a two-phase 6 equations system code using a 2D description of the vessel (or SFP pool) and a 1D meshing of circuits in a finite volume approach. It is implicitly coupled with the ICARE module to compute the heat transfers from the vessel structures to the fluid.

3.2 Representation of MIDI with ASTEC

The geometry of the ICARE module is based on imbricated axisymmetric objects, like cylinders in pressurized water reactors, but also squared objects like canisters in boiling water reactors or SFP racks. This last feature is used in the current work to represent the MIDI facility: the rectangular basin is represented by a squared structure with real fluid section (thus with deviation on the wet perimeter), containing two squared racks representing the set of grouped hot and cold racks, and a bypass channel. For each test, the hot rack and the cold rack contain the number of cylindric heating elements according to Table I, and their dimensions and surface are defined accordingly. This approach ensures a correct representation of the fluid section and porosities in hot and cold cells as well as in the bypass surrounding the racks, at the price of a small approximation on the area of the vertical surfaces delimiting the racks. The four loading patterns indicated in Figure 2 are thus simulated by the three configurations indicated in Figure 3 (as the ASTEC representation of two squares in a larger square could not be drawn in a satisfactory manner, the squares have been replaced by rectangles in the figure). It must be noticed that the loading patterns LP2 and LP4 are represented by the same ASTEC geometry since hot and cold racks are put all together.

The ASTEC axial nodalization (see Figure 3) is made of 2 meshes below the racks, 4 meshes inside the racks, and 9 meshes above. All elements of the pool (water and structures) are initiated at 50°C and a boundary condition imposes the atmospheric pressure at the top of the pool. Thermal losses along the basin are represented by a constant external temperature of 25°C associated to a heat exchange coefficient assessed from the energy balance of each test (average value 10 W/m^2/K).

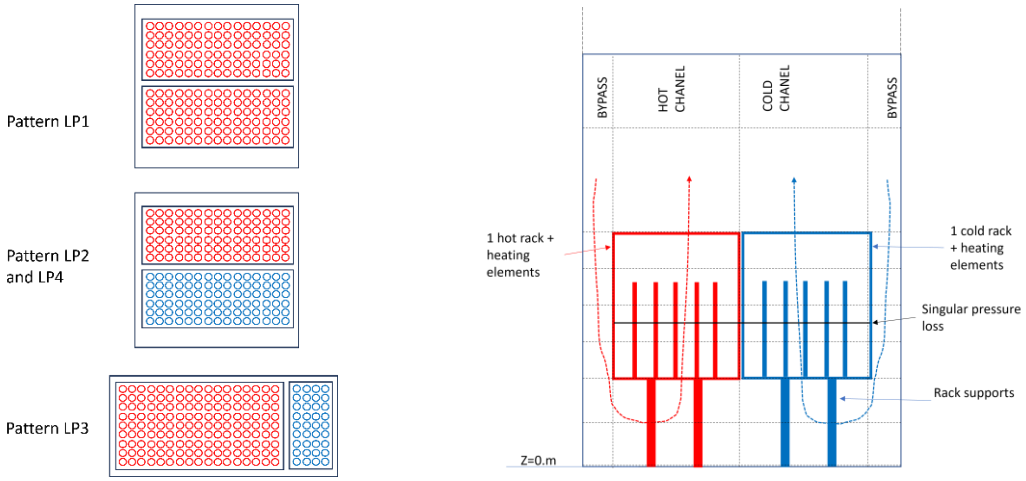

Figure 3: Representation of loading patterns in ASTEC (number of rods and cells geometry are not respected: cells are always squared in ASTEC) and scheme of the ASTEC meshing (upper basin part is not shown).

Table II: List of MIDI tests computed with ASTEC

Tests	Loading pattern (see Figure 2)	Overall heating power	Number of hot cells / Power in hot cells	Number of cold cells / Power in cold cells	Initial pool level
1_1	LP1	90.1 kW	21 / 4.3 kW	0 / 0 kW	4 m
2_1	LP2	92.2 kW	10 / 8.4 kW	11 / 0.7 kW	4 m
5_1	LP2	299.5 kW	10 / 27.3 kW	11 / 2.5 kW	4 m
7	LP2	300. kW	10 / 27.3 kW	11 / 2.5 kW	2 m
8	LP3	218.7 kW	4 / 50.0 kW	17 / 1.1 kW	4 m
9_0	LP3	55.0 kW	4 / 11.4 kW	17 / 0.6 kW	4 m

Since this simple geometry cannot take into account the complexity of the real geometry of the cells and the real fluid flowpath, the pressure losses along the cells are underestimated and must be corrected as they play a crucial role in such natural circulation flows. Indeed, mass flow rates obtained in test 1_1 without any additional pressure loss are too high by nearly a factor of 2. The calibration of the pressure loss is done once and for all using the test 1_1 where a uniform loading pattern was applied: a singular pressure loss is introduced in the cells, at mid-height of the heating structures, and the value of its coefficient k is adjusted to reproduce the measured mass flow rate obtained in the plateau of the test (see Figure 4). The obtained value $k=32$ has then been conserved for all other simulated tests.

3.3 Results of ASTEC V3.1.1 with Uniform Pattern

Results obtained with ASTEC V3.1.1 for test 1_1 after the calibration of the singular pressure drop are indicated in Figure 4. The evolution of the water inventory is well reproduced, indicating a correct energy balance and a good calibration of thermal losses which represent around 20% of the injected power.

The experimental outlet cell temperatures and mass flow rates have been averaged over the 21 cells, and the grey shaded area around the corresponding black curves represent the experimental standard deviation over the 21 cells. The initial temperature rise in the cell outlet is too fast in the ASTEC calculation, reaching 100°C in 8.7 h, to be compared with 11.9 h in the test. The mass flow rate evolution is also overestimated by ASTEC during this evaporation phase (while the pool stays subcooled, so up to 11.9 h). It is reminded that the mass flow rate during the plateau (from 11.9 h to 50 h) is fitted with ASTEC thanks to the calibration of the singular pressure drop. From 50 h, ASTEC predicts a strong increase of the mass flow rate due to the start of a boiling phase in the pool with the reduced hydrostatic pressure. This behaviour, not detected in the experiment, reveals the deficiency of the subcooled boiling model of ASTEC V3.1.1 applied to this configuration. The responsibility of the subcooled boiling model is checked by running ASTEC without any subcooled boiling model: in this case (blue lines in Figure 4), the final mass flow rate excursion is not predicted. This crucial point is studied in more details hereafter.

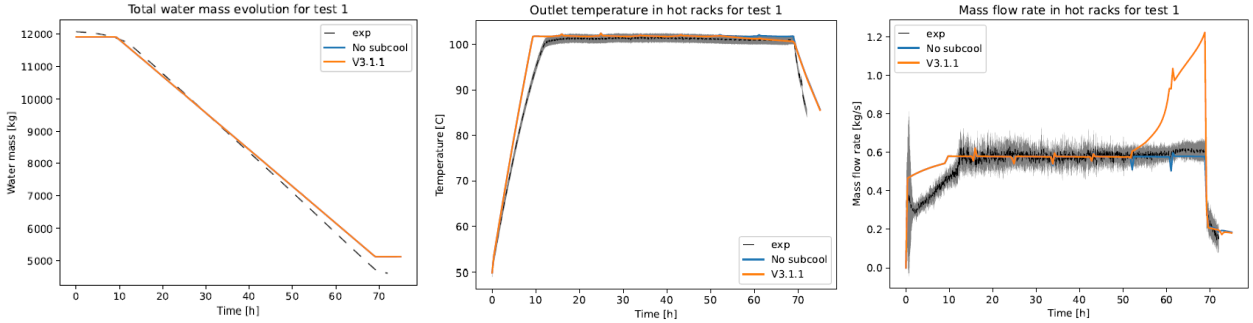

Figure 4: Evolution of pool water mass, temperature and mass flow rate, at the cell outlet in test 1. Grey shaded regions represent the uncertainties of experimental mass flow rate and temperature.

3.4 Introduction of Additional Subcooled Boiling Models in ASTEC

The modelling of subcooled boiling has been an intensive topic of research during the last decades. A review of such models is out of the scope of this paper but the reader can refer to [14, 15] for a short presentation of the topic. Most current models are based on the flux partitioning approach introduced by Kurul and Podowski [16, 17]. In this approach, the wall to fluid heat flux is partitioned between single-phase convection with liquid, quenching, and evaporation. The general expression of the evaporation term is:

$$Q_E = L_{LG}\,\rho_G\,\frac{\pi}{6}\,d_W^3 f N$$

where L_{LG} is the latent heat, ρ_G is the gas density, d_W is the bubble size at detachment, f is the bubble detachment frequency, and N is the nucleation site density. The last three parameters can be obtained from correlations established from dedicated experiments in specific conditions: pressure and heat flux range, pool boiling, forced convection, micro-channels…
The introduction of such correlations in CFD [18] or other thermal-hydraulic codes [19] has been reported to significantly improve the code predictions, in particular at low void fraction regimes. However, many of these correlations were established in conditions (pressure, subcooling, heat flux) close to in-reactor ones, whereas few studies have been performed in low pressure [20] and low heat flux conditions met in SFP.

In order to investigate the impact of such models on ASTEC modelling of MIDI tests, some recent or widely used subcooled boiling models adapted to pool boiling configurations have been introduced in ASTEC. Several ASTEC runs have been performed using models indicated in Table III, in addition to the previous cases presented in section 3.3.

Table III: Description of subcooled boiling models tested in ASTEC simulations of MIDI tests

Model name in ASTEC	**Origin of the model**	**Correlations used in Kurul and Podowski model**		
		d_W=bubbles size at detachment	**f = bubbles detachment frequency**	**N=nucleation site density**
No subcool	No subcooled boiling model: bubbles cannot appear if water is subcooled.	Not applicable		
V3.1.1	Model similar to Saha-Zuber [21] but fitted to KIT experimental data. Valid at P>2 bar.	Not applicable		
Lahey	Lahey [22] model with liquid enthalpy at bubble detachment from [21]. Used in TRACE V5 code [23].	Not applicable		
Unal-Cole	Kurul and Podowski [17]	[24]	[26]	[28]
Unal-BH	Kurul and Podowski [17]	[24]	[27]	[28]
TK-Cole	Kurul and Podowski [17]	[25]	[26]	[28]
TK-BH	Kurul and Podowski [17]	[25]	[27]	[28]

The results obtained on MIDI test 1_1 with each of these models introduced in ASTEC are presented in Figure 5 (water mass and temperatures at cell outlet are not displayed since all models lead to the results of Figure 4). It appears that the current V3.1.1 model leads to the largest deviation of mass flow rate, while the Lahey model seems to predict no subcooled boiling in this case. Other models based on Kurul and Podowski approach give intermediate results, with best predictions (among this family of models) for cases referred as “Unal-BH” and “TK-BH” which both use the bubbles detachment frequency from [27]. This better agreement could be expected since the Cole correlation [26] is simpler and depends only on gas and liquid densities and bubble detachment size, whereas the more recent correlation from Brooks and Hibiki [27] is based on 4 dimensionless parameters fitted with a large validation database.

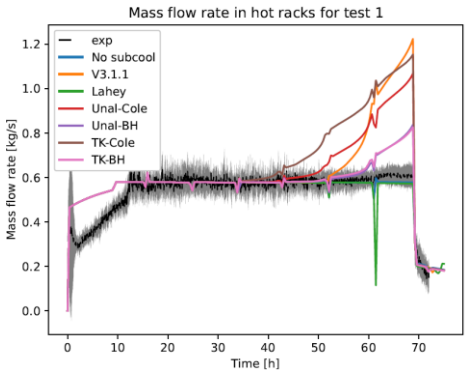

Figure 5: Comparison of several subcooled boiling models in ASTEC simulation of MIDI test 1_1.

3.5 Results with Different Patterns

The same process is now applied to other MIDI tests listed in Table II, investigating the influence of power levels, loading patterns and initial water level on the phenomenology. In all cases, the water level matches the experimental one and is not shown here. For most MIDI tests, the temperature at the cell outlet computed by ASTEC has the same behaviour as in Figure 4 which is model-independent. The exception is the test 8 which is the only test where the maximum power has been applied in hot cells: in this case, different levels of water subcooling can be observed in Figure 6 at the end of the heating phase (3 h). As expected, the calculation without any subcooled boiling model leads to the highest water temperature, corresponding to the saturation temperature at 3.2m below the water surface, i.e. 107°C. Consistently with the too strong subcooled boiling reported in section 3.4, the ASTEC V3.1.1 model computes subcooled boiling at too low temperatures, more than 2 degrees below the experimental value. Other models predict outlet temperatures close to experimental ones and within the measurement accuracy.

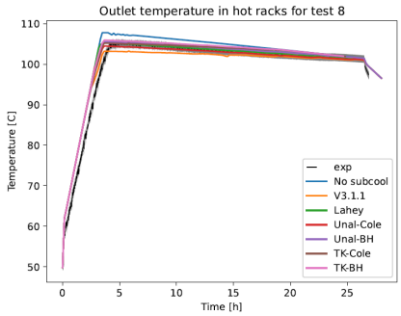

Figure 6: Evolution of temperature at the hot cell outlet in test 8.

Mass flow rates in hot and cold cells obtained for each test and model are indicated in Figure 7. At first look, ASTEC is able to capture the increase of the mass flow rate in hot cells with increasing power. It can also be remarked that the agreement with experimental results increase with the power level in hot cells: best and worst results are obtained with tests 8 and 9_0 respectively, corresponding to the highest power in hot cells and lowest overall power. This can be explained by the thermal influence of hot cells on neighboured cold ones in the experiment, while there is not direct heat exchange between hot or cold cells in ASTEC calculations. From this point of view, test 8 is best reproduced thanks to the limited influence between hot and cold cells due to the loading pattern. This thermal influence, not represented in ASTEC, also explains the fact that hot cell flows are always overestimated by ASTEC while cold flows are always underestimated (except in test 2 where the measured cold mass flow rate is below the 0.5kg/s sensitivity of the sensor).
Looking at the different subcooled boiling models, it appears from hot cell flows evolution that best overall results are obtained with Lahey and TK-BH models. More precisely, the Lahey model looks very well

adapted to low heat fluxes (tests 2_1 and 9_0), while the TK-BH model gives better predictions at higher heat flux (tests 5_1,7 and 8). Again, this must be related with the range of parameters that were considered when building these correlations. In particular, it has been identified that the Jakob number reached in test 8 (highest heat flux of 50 kW/m^2) was close to 1.0x10^{-3}, which is an order of magnitude smaller than the lower bound of the Brooks and Hibiki [27] correlation for bubble detachment frequency. Other tests with lower heat flux have even lower Jakob number, hence a weaker agreement.

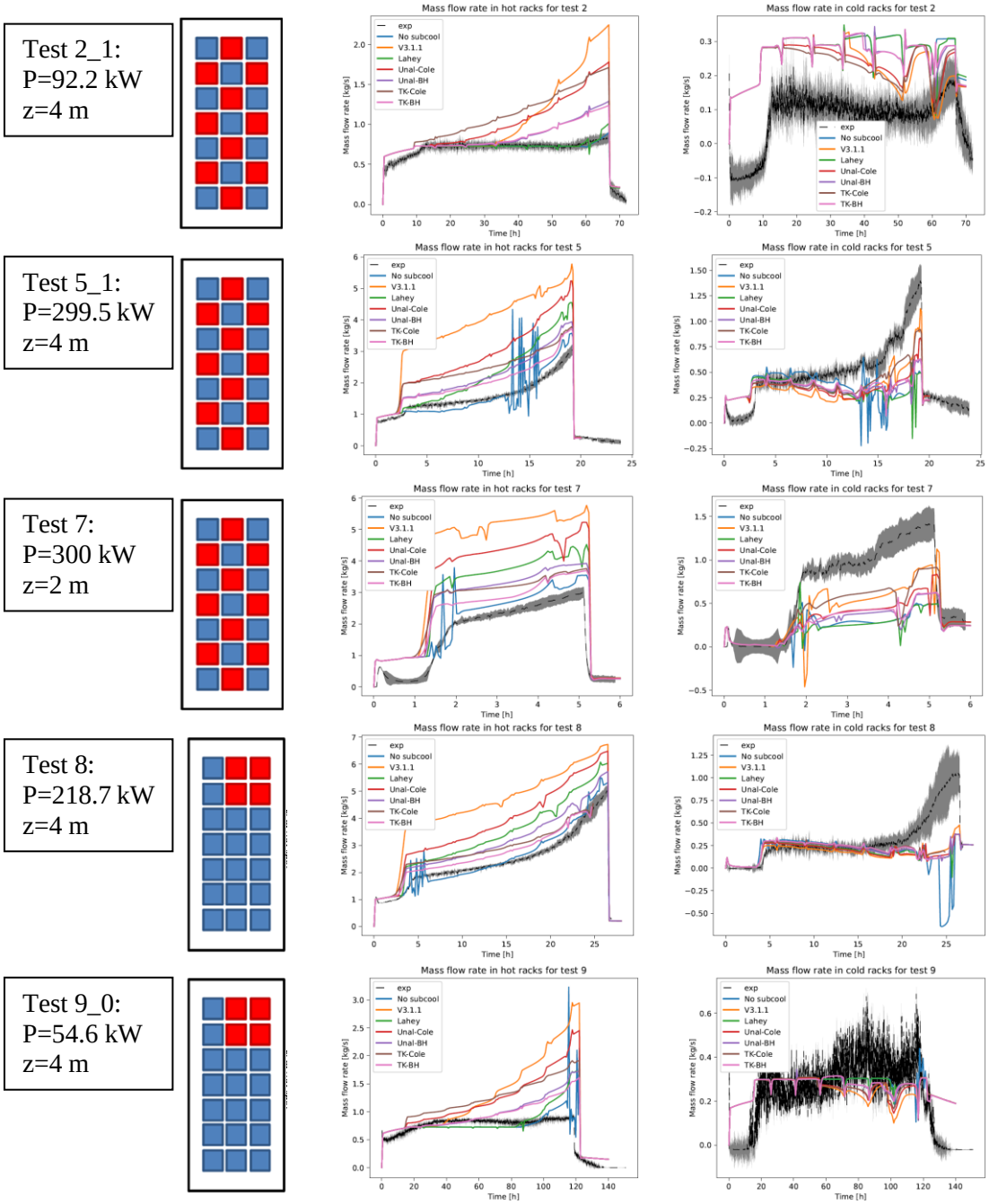

Figure 7: Mass flow rates in hot (left) and cold (right) cells for 5 MIDI tests.

3.6 Alternative ASTEC Modelling using Weighted Channels

In order to provide ASTEC users with modelling best-practices, an alternative modelling of the MIDI tests has been tested. Instead of grouping all together hot racks and cold racks in two large racks, a single hot rack and a single cold rack are represented, with their real geometry, but with a weight corresponding to the number of hot and cold racks of each test. Actually, this approach looks more natural than the previous one but was not yet validated against dewatering tests, by lack of experimental data. Simulations of same MIDI tests, with same subcooling models, have produced very similar results as the ones exposed in previous section, with similar CPU time, thus validating that both approaches were equivalent. As an illustration, hot cells mass flow rate from test 8 are indicated for the previous grouped (left) and weighted approach (right).

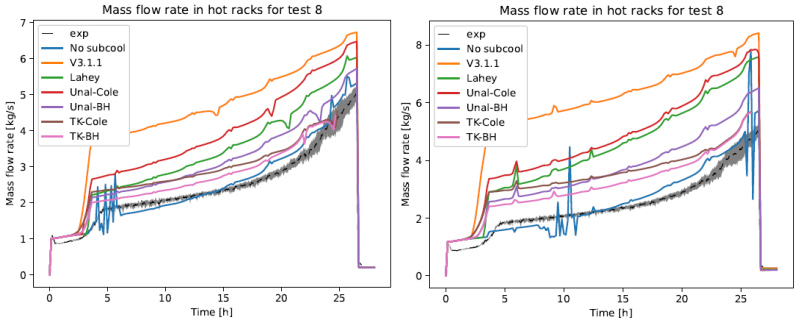

Figure 8: Hot cells mass flow rate from test 8 for the grouped (left) and weighted approach (right).

3.7 Numerical aspects

Figure 7 and Figure 8 indicate that best results are obtained without any subcooling models. However, such simulations are not satisfactory for two reasons: first because of numerical issues related to the violent water vaporization when saturation is reached, leading to very small time steps, and second to associated possible reverse flows (not observed experimentally) as for instance on cold racks mass flow rate on test 8.

In addition to models improvement, one of the objective of this work was to study some numerical issues previously reported during SFP dewatering [9]: due to the different wall to fluid heat flux models applied when a mesh is nearly full of water or nearly empty, some discontinuities appear when the water level switches from an axial level to a lower one. During fuel assemblies uncovery, things can get worse since these discontinuities can have a strong impact on the flow (sudden vaporization), and hence on the fuel cladding temperature which suddenly drops. Such behaviour can also be observed here on mass flow rate evolutions, for instance in case V3.1.1 of Figure 8 with the weighted approach (equidistant small peaks) and on-going activities are focused on the reduction of these features, thanks to MIDI validation data. This topic will be also further studied in ASPIC tests (assembly dewatering, [10]) modelling that will start in 2024.

4 CONCLUSION AND PERSPECTIVES

Simulations of MIDI tests have been performed with ASTEC to assess the capability of the code to predict natural circulation flows occurring during a SFP dewatering transient. It was shown that current V3.1.1 model, validated for high pressures, predicts a too intense subcooled boiling in the racks which leads to mass flow rates much higher than in the experiment. Several subcooled boiling models from the literature have been tested to improve the results. Best agreement was found with models referred as Lahey and TK-BH for low and high heat flux respectively. Additional investigations are ongoing to further improve the results, like introducing a model of temperature for the onset of nucleate boiling. Further works are also needed to correct numerical issues related to the axial nodalization.

This work confirms that such system codes can be used for first order calculations of natural circulation in open regions, provided that singular pressure losses in the heated region can be characterized.

However, it must be stressed that the validity of the flows computed by ASTEC above the racks is still to be assessed: the uniform temperature field observed in the experiment was reproduced by ASTEC, indicating an efficient mixture of the fluid, but this is not sufficient to really assess the predicted flow which may be too intense. In the near future, ASTEC calculations will be compared to results of the SATURNE-CFD code in order to check the validity of the flow computed by ASTEC in the pool region.
It is also planned to model with ASTEC the ASPIC experimental tests, related to the second axis of the DENOPI project and dedicated to the uncovery of a SFP assembly in its storage cell with or without spray to check the coolability of an assembly. Then, additional tests will also be run in MIDI and ASPIC within the new project POLCA launched by OECD in 2024 to consolidate these validation tasks. Benchmark activities involving different thermal-hydraulics codes will also be conducted. Beyond SFP activities, these works also provide relevant data for the understanding of large natural convection loops that are expected in immersed passive heat removal systems of Small Modular Reactors that ASTEC should address.

5 ACKNOWLEDGMENTS

The authors wish to thank S. Morin, J. Martin, G. Brillant and P. Ruyer for fruitful discussions in preparing this work. The present work has been performed using part of the experimental results of DENOPI research program on SFP-LOCA ended in 2022. The French Government and the National Research Agency are gratefully acknowledged for their interest and financial support (contract reference: ANR 11 – RSNR 006).

6 REFERENCES

1. OECD NEA, "*Phenomena Identification and Ranking Table. R&D Priorities for Loss-Of-Cooling and Loss-Of-Coolant Accident in Spent Nuclear Fuel Pools*", Report NEA n°7443 (2018).
2. J. Martin, N. Trégourès, "OECD/NEA R&D priorities for loss-of-cooling and loss-of-coolant accidents in Spent-Fuel-Pools", *Nuclear Engineering and Design*, **410** 112380, ISSN 0029-5493 (2023), https://doi.org/10.1016/j.nucengdes.2023.112380.
3. S.R. Chen, W.C. Lin, Y.M. Ferng, C.C. Chieng, B.S. Pei, "CFD simulating the transient thermal–hydraulic characteristics in a 17×17 bundle for a spent fuel pool under the loss of external cooling system accident", *Annals of Nuclear Energy*, **73**, pp. 241-249, ISSN 0306-4549 (2014), https://doi.org/10.1016/j.anucene.2014.06.054.
4. Ronald Oertel, T. Hanisch, E. Krepper, D. Lucas, F. Rüdiger, J. Fröhlich, "Two-scale CFD analysis of a spent fuel pool involving partially uncovered fuel storage racks", *Nuclear Engineering and Design*, **341**, pp. 432-450, ISSN 0029-5493 (2019), https://doi.org/10.1016/j.nucengdes.2018.10.014.
5. T. Someya, H. Chitose, S. Watanabe, Y. Nemoto, Y. Kaji, "Study on Loss-of-Cooling and Loss-of-Coolant Accidents in Spent Fuel Pool (8)Safety Margin of Spent Fuel in Large LOCA Event by the Simple Assessment Method", *The Proceedings of the International Conference on Nuclear Engineering (ICONE)*, Vol.2019.27, pp.1153, (2019), https://doi.org/10.1299/jsmeicone.2019.27.1153.
6. A. Kaliatka, A. Graževičius, T. Kaliatka, "Analysis of loss of cooling accidents in the spent fuel pools using system thermal hydraulics and computational fluid dynamic codes", *Nuclear Engineering and Design*, **412** 112447,ISSN 0029-5493 (2023), https://doi.org/10.1016/j.nucengdes.2023.112447.
7. S. Carlos, F. Sanchez-Saez, S. Martorell, "Use of TRACE best estimate code to analyze spent fuel storage pools safety", *Progress in Nuclear Energy*, **77**, pp. 224-238, ISSN 0149-1970 (2014), https://doi.org/10.1016/j.pnucene.2014.07.008.
8. J-A Zambaux, L. Laborde and P. Ruyer, "Calculating steam-water flows at large non-condensible gas concentration with severe accident code ASTEC V2.2", *Proceedings of the 19th International Topical Meeting on Nuclear Reactor Thermal Hydraulics (NURETH-19)*, Brussels, Belgium (2022).
9. O. Coindreau, L.E. Herranz, R. Bocanegra, S. Ederli, P. Maccari, F. Mascari, O. Cherednichenko, A. Iskra, P. Groudev, P. Vryashkova, P. Petrova, A. Kaliatka, V. Vileiniškis, M. Malicki, T. Lind, O. Kotsuba, I. Ivanov, F. Giannetti, M. D'Onorio, P. Ou, L. Feiye, P. Piluso, Y. Pontillon, M. Nudi,

"Uncertainty quantification for a severe accident sequence in a SFP in the frame of the H-2020 project MUSA: First outcomes", *Annals of Nuclear Energy*, **188** 109796 (2023).
10. B. Migot, G. Brillant, J. Martin and S. Morin, "DENOPI project devoted to spent fuel pool accidents: overview on the thermal hydraulics experimental facilities", *Proceedings of the 19th International Topical Meeting on Nuclear Reactor Thermal Hydraulics (NURETH-19)*, Brussels, Belgium (2022).
11. L. Chailan, L. Bosland, L. Carénini, J. Chambarel, P. Chatelard, F. Cousin, P. Drai, G. Kioseyian, S. Phoudiah, V. Topin, "Overview of ASTEC integral code status and perspectives", *Proceedings of the 9th European Review Meeting on Severe Accident Research (ERMSAR-2019)*, Prague, Czech R., (2019).
12. P. Chatelard and L. Laborde, "ASTEC V2.2 code validation: Illustrative results and main outcomes", *Nuclear Engineering and Design*, **413** 112547, ISSN 0029-5493 (2023), https://doi.org/10.1016/j.nucengdes.2023.112547.
13. T. Glantz, T. Taurines, O. De Luze, S. Belon, G. Guillard, F. Jacq, "DRACCAR: A multi-physics code for computational analysis of multi-rod ballooning, coolability and fuel relocation during LOCA transients Part one: General modeling description", *Nuclear Engineering and Design*, **339**, pp. 269-285, ISSN 0029-5493 (2018), https://doi.org/10.1016/j.nucengdes.2018.06.022.
14. A. Rabhi, "*Numerical Modelling of Subcooled Nucleate Boiling for Thermal Management Solutions Using OpenFOAM*", Licentiate Thesis, Mälardalen University, School of Business, Society and Engineering, Future Energy Center (2021).
15. H. Hoang, I. C. Chu, D. J. Euh, and C. H. Song, "On the Application of Wall Boiling Models to prediction of subcooled flow boiling using EAGLE code", *Proceedings of the 16th International Topical Meeting on Nuclear Reactor Thermal Hydraulics (NURETH-16)*, Chicago, USA (2015).
16. N. Kurul and Michael Z. Podowski. "Multidimensional effects in forced convection subcooled boiling." *International Heat Transfer Conference Digital Library*. Begel House Inc. (1990).
17. N. Kurul. "On the modeling of multidimensional effects in boiling channels.", *ANS. Proc. National Heat Transfer Con. Minneapolis*, Minnesota, USA (1991).
18. E. Krepper and R. Rzehak, "CFD for subcooled flow boiling: Simulation of DEBORA experiments", *Nuclear Engineering and Design,* **241** (9), pp. 3851-3866, ISSN 0029-5493 (2011). https://doi.org/10.1016/j.nucengdes.2011.07.003.
19. V. Kumar and R. K. Salko Jr, "Implementation of a new wall boiling model in CTF", *ANS Winter Meeting and Nuclear Technology Expo 2020*, Chicago, USA, Vol. 123, 1728-1731 (2020).
20. J.Y. Tu, G.H. Yeoh, "On numerical modelling of low-pressure subcooled boiling flows", *International Journal of Heat and Mass Transfer*, **45** (6), pp. 1197-1209, ISSN 0017-9310 (2002), https://doi.org/10.1016/S0017-9310(01)00230-7
21. P. Saha and N. Zuber, "Point of net vapor generation and void fraction in subcooled boiling", *Proceedings of the 5th International Heat Transfer Conference*, Tokyo, Japan, Vol. 4, 175-179 (1974).
22. R. T. Lahey, Jr., "A Mechanistic Subcooled Boiling Model", *Proceedings of the 6th International Heat Transfer Conference*, Toronto, Canada, Vol. 1, 293-297 (1978).
23. US NUCLEAR REGULATORY COMMISSION, "*TRACE V5.840 Theory Manual: Field Equations, Solution Methods, and Physical Models*", Tech. rep., US Nuclear Regulatory Commission (2013).
24. H.C. Unal, "Maximum bubble diameter, maximum bubble growth time and bubble growth rate", *Int. J. Heat Mass Transfer*, **19**, pp. 643-649 (1976).
25. V.I. Tolubinsky and D.M. Kostanchuk, "Vapour bubbles growth rate and heat transfer intensity at subcooled water boiling". *Proceedings of the 4th International Heat Transfer Conference*, Paris-Versailles, France, Vol. 23. (1970).
26. R. Cole, "A photographic study of pool boiling in the region of the critical heat flux". *AIChE Journal*, **6** (4), pp. 533–538 (1960).
27. C.S Brooks and T. Hibiki, "Wall nucleation modeling in subcooled boiling flow". *International Journal of Heat and Mass Transfer*, **86**, pp. 183–196 (2015).
28. M. Lemmert and J.M Chawla, "Influence of flow velocity on surface boiling heat transfer coefficient", *Heat Transfer in Boiling*, pp. 237–247, Academic Press and Hemisphere, New York and Washington DC (1977).